Meccanica (2007) 42:451–463
DOI 10.1007/s11012-007-9064-8

Assessing joint angles in human hand via optical tracking device and calibrating instrumented glove

M. Veber · T. Bajd · M. Munih

Received: 26 July 2006 / Accepted:25 January 2007 / Published online: 2 June 2007

Abstract The aim of this paper is to present a method for assessing joint angles in a human hand: a method suitable for the calibration of an instrumented glove. The method is based on an optical tracking device and an inverse-kinematic model of the human hand. It requires only one reflective marker to be attached to each finger and three on the dorsal aspect of the hand in order to assess angles in finger joints. A further three markers are needed to calculate angles in thumb joints. Joint angles assessed through inverse kinematics and with the calibrated glove were validated against reference angles calculated from the centers of rotation of the joints while measuring the finger movements with multiple markers. In fingers, the mean difference between the reference angles and the angles assessed by the glove did not exceed $\pm 7^\circ$ when the proposed model-based method was used to calibrate the glove. For the thumb the mean error did not exceed $\pm 5^\circ$ when the reference method was used to calibrate the glove.

Keywords Finger joint angles · Kinematic model of the hand · Instrumented glove · Calibration

Abbreviations

D-H	Denavit-Hartenberg
DOF	Degrees of freedom
MCP	Metacarpophalangeal joint
PIP	Proximal interphalangeal joint
DIP	Distal interphalangeal joint
CMC	carpometacarpal joint
IP	Interphalangeal joint
CoR	Center(s) of rotation
f-e	Flexion–extension
ab-ad	Abduction–adduction

M. Veber (✉) · T. Bajd · M. Munih
Faculty of Electrical Engineering, Laboratory of Robotics and Biomedical Engineering, University of Ljubljana, Trzaska c.25, 1000 Ljubljna, Slovenia
e-mail: veberm@robo.fe.uni-lj.si

1 Introduction

The human hand is a versatile system with 25 degrees of freedom [15]. The incredible adaptability of the human hand to specific requirements raises the question of how the joints are controlled in order to perform so many different tasks. In contrast to many studies related to the control of joints of multi-fingered robotic grippers [3,17,14], studies related to the task-oriented control of joints in a human hand are scarce because a generally accepted approach for accurate noninvasive assessment of hand kinematics is not available.

The aim of this paper is to propose a method based on an optical tracking system and an inverse-kinematic model of the human hand that calculates joint angles in thumb and fingers from the positions of a small number of reflective markers attached to the surface of the hand. The method will be applied to the calibration of an instrumented glove, which is intended to be used as a complementary system overcoming the main drawback of the optical tracking system — occlusion of markers

during manipulative tasks. The proposed method and the calibrated glove will be compared with reference methods [23,6,16] that require a larger set of markers in order to assess angles in thumb and finger joints.

Optical tracking is a well-established technique [12] that does not hinder the movement of the human body as for instance exoskeletons. It enables the measurement of body kinematics by tracking reflective markers placed over bony landmarks. Because of its accuracy, the method can be considered as a reference for reconstruction of kinematics. The body's kinematics are modeled by rigid bodies linked with joints. In general, three noncollinear markers have to be attached to each rigid body to reconstruct its motion in 3D.

The difficulty in capturing hand kinematics originates from the relatively large number of degrees of freedom concentrated in a very small place [16]. This problem can be to some extent reduced by considering the characteristic patterns of finger motion, so that fewer markers can be used. Skin artifacts that are large compared with the distances between markers can make the reconstruction of a frame attached to a phalange even more difficult. In addition, the range of motion of some joints is very small.

Another drawback of optical tracking is the occlusion of markers. This deficiency becomes even more obvious with a large number of markers and is the main reason why optical tracking systems are not widely used for the assessment of hand kinematics. In magnetic tracking systems there is no problem with occlusion, but in currently available commercial systems markers are too big to be attached appropriately to fingers or else only the use of a small number (usually one or two) of markers is supported. There is also a problem of interference from the environment in some magnetic tracking systems.

Finger kinematics can also be assessed by instrumented gloves, which have been used in many experiments [19]. However, in most cases the raw data from the gloves were used. For instance, in one study an instrumented glove was used when analyzing grasping sequences by hidden Markov models [2]. A similar problem was solved elsewhere with fuzzy-logic decision functions [1]. In such experiments where a glove is used, significant effort is devoted to compensating for the offset in the raw response, which occurs when the bend sensors are fully extended. This offset is not repeatable for different attachments, not even when used with the same hand. By carrying out a set of specific hand movements, an estimate of offset can be provided and the active range of analog-to-digital converters established. For a hand with a known range of finger-joint motions, rough estimates of the time courses of joint angles could be obtained [20] if the responses of the bend sensors were linear. We are not aware of any article comparing angles in finger joints assessed using an instrumented glove with the angles obtained by using a reliable reference method. Glove repeatability was studied by Dipietro et al. [8], where errors related to donning and doffing were analyzed, although only for specific postures. In another study [22], a glove mounted on an artificial hand was calibrated. This study provided a good estimate of the glove accuracy; but because a model, instead of a real human hand, was used in the experiment, some errors such as skin movement artifacts were not taken into account. It is also important to note that this approach could not be used for calibration of a glove in human applications where the kinematics of hands with diverse properties are to be assessed.

The paper begins by presenting a kinematic model of the human hand, which can be scaled according to the hand's external dimensions. In the sections that follow, methods are presented for assessing angles in finger joints through inverse kinematics and from the centers of rotation (CoR) of joints. Both methods are applied to the calibration of an instrumented glove. Finally, the angles assessed through the use of inverse kinematics and with the calibrated glove are compared with the reference angles calculated from the CoR of joints.

2 Methods

2.1 Kinematic model of the hand

Finger and thumb kinematics were described with Denavit–Hartenberg notation (D-H) [7]. The coordinate frames placed according to the rules stated by D-H are presented in Fig. 1. The z-axis of a frame attached to the wrist is aligned with the middle finger.

Four degrees of freedom (DOF) are used to describe each finger [21]: two for the metacarpophalangeal joint (MCP), flexion–extension (f-e) and abduction–adduction (ab-ad); and two for the proximal interphalangeal (PIP) and the distal interphalangeal (DIP) joint f-e. It has been shown that five DOF are necessary to model key kinematic features of the human thumb [5].

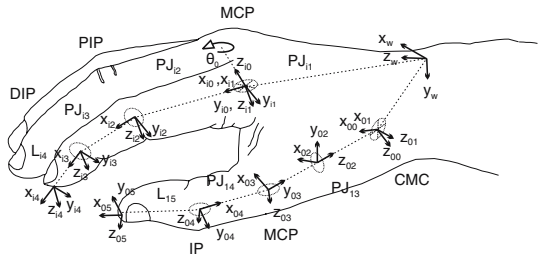

Fig. 1 Finger joints used in a kinematic model of a finger and the thumb

Table 1 Denavit–Hartenberg parameters for the hand model

Thumb ($i = 1$)			
Θ	d	a	α
Θ_{i1}	0	0	$-\pi/2$
$\Theta_{i2} + \pi/2 + \epsilon_{i2}$	0	0	$-\pi/2$
Θ_{i3}	$-PJ_{i3}$	0	$-\pi/2 - \alpha_{i3}$
$\Theta_{i4} + \pi/2$	0	$-PJ_{i4}$	0
$\Theta_{i5} + \pi$	0	L_{i5}	0
Fingers ($i = 2, 3, 4, 5$)			
Θ_{i1}	0	0	$-\pi/2$
Θ_{i2}	0	PJ_{i2}	0
Θ_{i3}	0	PJ_{i3}	0
Θ_{i4}	0	L_{i4}	0

However, the axes of rotation in the thumb are neither perpendicular nor parallel and are nonintersecting. Our model of the thumb comprises a universal joint and two hinge joints. The first two DOF represent f-e and ab-ad of the carpometacarpal (CMC) joint; the third DOF enables fingerpad opposition; while the remaining two DOF represent f-e of the MCP and interphalangeal (IP) joints.

The D-H parameters are collected in Table 1. In the case of fingers, parameters PJ_{i2} ($i = 2, 3, 4, 5$) denote the distances from the ith MCP joint to the PIP joint, PJ_{i3} the distance from the PIP to the DIP joint, and L_{i4} the length of the ith distal phalanx. In the thumb ($i = 1$), PJ_{i3} denotes the distance from the CMC joint to the MCP joint, PJ_{i4} the distance from the MCP to the IP joint and L_{i5} the length of the distal phalanx. Parameters α_{i2} and ϵ_{i3} define the initial configuration of the thumb at $\Theta_{i1}, \ldots, \Theta_{i5} = 0$. The initial configuration of the hand corresponds to the hand flat with the sides of fingers touching and with the fully abducted thumb.

The capitate bone was selected as the origin of the hand model. The base frame $j = 0$ of the ith finger ($i = 2, 3, 4, 5$) was attached to the CoR of the ith MCP joint. The transformation from the origin of the hand model to the ith finger base is described within Eq. 1. PJ_{i1x} and PJ_{i1z} denote the position of the ith MCP joint relative to the wrist frame, while s_i and c_i denote the trigonometric functions $\sin\varphi_i$ and $\cos\varphi_i$, where $\varphi_1 = -\pi/2$ and $\varphi_2 = \pi$.

$$\mathbf{T_{w0i}} = \begin{bmatrix} 1 & 0 & 0 & PJ_{i1x} \\ 0 & 1 & 0 & 0 \\ 0 & 0 & 1 & PJ_{i1z} \\ 0 & 0 & 0 & 1 \end{bmatrix} \begin{bmatrix} c_1 & 0 & s_1 & 0 \\ 0 & 1 & 0 & 0 \\ -s_1 & 0 & c_1 & 0 \\ 0 & 0 & 0 & 1 \end{bmatrix} \begin{bmatrix} 1 & 0 & 0 & 0 \\ 0 & c_2 & -s_2 & 0 \\ 0 & s_2 & c_2 & 0 \\ 0 & 0 & 0 & 1 \end{bmatrix} \quad (1)$$

The base of the thumb was positioned to the CoR of the CMC joint. F-e and ab-ad axes of the CMC joint were determined according to Ref. [13] as follows. The f-e axis was defined as passing through the CMC joint and a point translated along the y_w axis (Fig. 1) for 20 mm from the MCP joint of the ring finger. The ab-ad axis of the CMC joint was defined as being normal to the plane defined by the thumb metacarpal bone in the neutral position and the f-e axis of the CMC joint.

The main advantage of the proposed model over existing models described in the literature is its scaling according to the external dimensions of the human hand (its length and width) through scaling factors known from statistical anthropometry [4]. The hand length was measured on the palmar aspect of the hand from the distal crease at the wrist to the tip of the middle finger. The palm width was measured from the edge of the hand on one side, across the palm, to the edge of the hand at the level of MCP joints on the other side, with fingers parallel and fully extended. The hand length and width of the subject who took part in this study were 204 and 90 mm, respectively.

2.2 Measurement set-up

A motion tracking system (OptoTrak®, Northern Digital Inc.) was used to validate kinematic parameters and to calibrate an instrumented glove (DataGlove® Ultra Series, 5DT Inc., 14 DOF). OptoTrak can accurately measure the three-dimensional position of infrared markers placed in front of the system of three cameras, with an accuracy of 0.1 mm. The relative positions and orientations of the cameras are fixed, so the exact coordinates of each marker can be calculated from the

known geometry of the camera set-up. The system is calibrated before each measurement session with the help of a calibration plate having eight embedded markers. The position and orientation of the plate placed in front of the cameras define the coordinate system in which marker positions are expressed.

A DataGlove has 14 fiber-optic bend sensors that measure f-e angles in the MCP and PIP joints as well as ab-ad angles between fingers. Two sensors are used to measure f-e angles of the thumb IP and CMC joints, while one sensor measures the ab-ad angle of the thumb. The system interfaces with the computer via a USB port. It features a 12-bit analog-digital converter, but the resolution of the optical bend sensors is much smaller, typically below 10 bits.

Thumb, index, and middle-finger kinematics of one subject, free from musculoskeletal disorders, were considered. Two sets of cameras facing in opposite directions were used in the investigation. Infrared markers were attached to the anatomical landmarks of the CMC, MCP, PIP, DIP, and IP joints of thumb, index, and middle finger and on the fingertips, as presented in Fig. 2. One marker was attached above the capitate bone. The data from the motion tracking system and instrumented glove were recorded simultaneously at a sampling rate of 60 Hz.

2.3 A reference method for assessing angles in finger joints

Joint angles estimated from the CoR of joints can be considered as the gold standard in noninvasive assessment. General methods used to determine axes of rotation and CoR of joints of lower or upper extremities

Fig. 2 Measurement set-up: instrumented glove and infrared markers attached to anatomical landmarks above the CMC, MCP, PIP, DIP, and IP joints, to the capitate bone, and on the fingertips

[9,10] are not appropriate for fingers. Satisfactory results can be obtained when markers are separated as far as possible from each other. This can be achieved by using a small set of markers. The 3D-parameter estimation problem for the PIP and DIP joints was simplified to a 2D problem as proposed in Refs. [23] and [16] and presented in Fig. 3a. The same approach was also used to estimate the CoR of the MCP and IP joints of the thumb. In this way, we obtained a planar solution, defined by markers $\mathbf{m_{PIP}}$, $\mathbf{m_{DIP}}$, and $\mathbf{m_{FT}}$, which were attached above the PIP and DIP joints and on the fingertip. We minimized the cost function C [23] to obtain the parameters for estimating the locations of the PIP and DIP joints:

$$C = \sum_{k=1}^{N} \left((D_{\mathrm{PIP}k} - D_{\mathrm{PIP}})^2 + (D_{\mathrm{DIP}k} - D_{\mathrm{DIP}})^2 \right). \quad (2)$$

Parameters D_{PIP} and D_{DIP} denote the optimal depths of PIP and DIP joints below the position of the surface markers $\mathbf{m_{PIP}}$ and $\mathbf{m_{DIP}}$, while $D_{\mathrm{PIP}k}$ and $D_{\mathrm{DIP}k}$ represent the distances from markers $\mathbf{m_{PIP}}$ and $\mathbf{m_{DIP}}$ to the CoR of PIP and DIP joints, calculated for the kth frame. N stands for the number of all frames. The cost function C was slightly modified. If there are many samples recorded for a specific posture as compared with other postures, perhaps because the motion was stopped for a while in that posture, then the cost function is biased. This effect can be reduced by using a weighted average, where weights w_k are calculated from the relative frequencies of angle $(\Theta_k + \Psi_k)$.

L_{mid} and L_{dist} in Fig.3a denote the lengths of middle and distal phalanges, and $\mathbf{m_{MCP}}$ is the position of the marker attached above the MCP joint. The minimum of the cost function was obtained by the Newton gradient method, subjected to linear constraints. The distances L_{dist}, L_{mid}, D_{DIP}, and D_{PIP} were varied for each step of the optimization. They were used to calculate the position of PIP and DIP joints in the reference frame as an intersection of two arcs with radii L_{dist} and D_{DIP} for DIP, and L_{mid} and D_{PIP} for PIP joints, as shown in Fig. 3a. For all other frames, the positions of the PIP and DIP joints were transformed into standstill points with respect to the coordinate frames attached to the proximal ($\mathbf{H_{PROX}}$) and middle ($\mathbf{H_{MID}}$) phalanges. In this way we were able to calculate $D_{\mathrm{PIP}k}$ and $D_{\mathrm{DIP}k}$ for all other frames. The initial values of parameters L_{dist} and L_{mid} were acquired from the positions of markers, while D_{DIP} and D_{PIP} were obtained from measurements of finger thickness at the level of the PIP and DIP

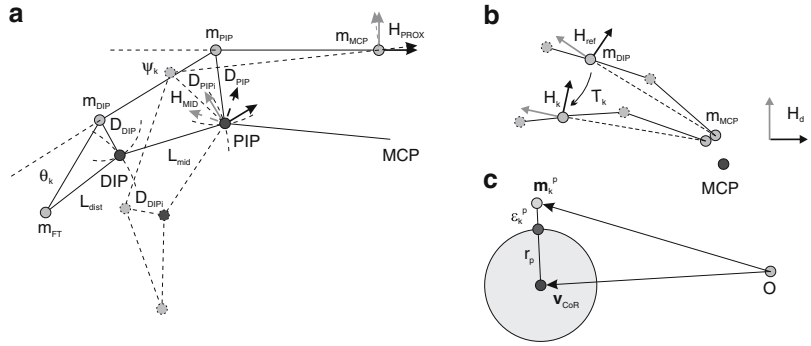

Fig. 3 Assessment of centers of rotation of the PIP and DIP joints of fingers and the MCP and IP joints of the thumb [23] (**a**), MCP joints of fingers [16] (**b**), and CMC joint of the thumb [6] (**c**)

joints. The constraints guaranteed that the optimization routine would be able to cope with each posture.

For the MCP joint, improved results can be obtained by using the marker $\mathbf{m_{PIP}}$, which is distant from the joint [16]. We modified the proposed method, as shown in Fig. 3b. The PIP joint was kept motionless (indicated by a dotted line). The orientation of the coordinate frame ($\mathbf{H_{ref}}$) was reconstructed for the reference frame from the positions of markers $\mathbf{m_{MCP}}$ and $\mathbf{m_{DIP}}$ attached to the observed finger, and from the marker attached to the MCP joint of the adjacent finger. $\mathbf{H_{ref}}$ was positioned to the location of $\mathbf{m_{DIP}}$. The CoR of MCP joint was found by minimizing the cost function defined as follows [16]:

$$C = \sum_{k=1}^{N} w_k \|\mathbf{T_k}\mathbf{C}_{\mathrm{MCP}} - \mathbf{C}_{\mathrm{MCP}}\|. \tag{3}$$

$\mathbf{T_k}$ denotes a transformation matrix that moves the coordinate frame ($\mathbf{H_{ref}}$) from the initial ($k = 1$) to the kth ($k = 2, \ldots, N$) pose, while ($\mathbf{C_{MCP}}$) represents a point that is invariant to transformations ($\mathbf{T_k}$) and can therefore be taken for the CoR of the MCP joint. The CoR of MCP joints were expressed relative to the coordinate frame of the hand dorsum ($\mathbf{H_d}$). The weights w_k in the cost function were included for reasons similar to those for estimating the CoR of PIP and DIP joints. The w_k were estimated from the relative frequencies of ($\mathbf{H_k}$) rotation with respect to ($\mathbf{H_d}$).

The average CoR of the CMC joint was estimated by minimizing a cost function C that assumes that P markers attached to the carpal bone maintain a constant distance r^p from the CoR of the CMC joint ($\mathbf{v_{CoR}}$) (Fig. 3c):

$$C = \sum_{p=1}^{P}\sum_{k=1}^{N}\left(\sqrt{\mathbf{m_k^p} - \mathbf{v_{CoR}}} - r^p\right)^2. \tag{4}$$

The spherical fit should have minimal variation ϵ_k^p in the separation length between the CoR of the CMC joint and the pth marker position $\mathbf{m_k^p}$ at the kth frame, for all k ($k = 1, \ldots, N$).

In Ref. [6] an optimal closed-form solution to this problem is provided, where the constrained least-squares solution is obtained by using a carefully chosen normalization scheme. The method performs well even for joints with small ranges of motion.

The parameters for the reconstruction of the CoR of joints in the fingers ($\mathbf{C_{MCP}}$, L_{dist}, L_{mid}, D_{DIP}, and D_{PIP}) were estimated from the signals recorded for f-e of the MCP joints with extended PIP and DIP joints, and f-e of PIP and DIP joints at fixed f-e in MCP joints. The CMC joint was kept motionless when assessing parameters for reconstructing the MCP and IP joints of the thumb (L_{prox}, L_{dist}, D_{MCP}, and D_{IP}). The CoR of the CMC joint was estimated from circumduction of the thumb.

2.4 A method for assessing angles through inverse kinematics

Joint angles in fingers were obtained by solving the inverse-kinematics problem of a two-link manipulator [18]. Angles related to the ab-ad and f-e angles in the MCP and f-e angles in the PIP joints were obtained from the known position of a marker attached above the DIP joint. In human fingers, the movement of PIP

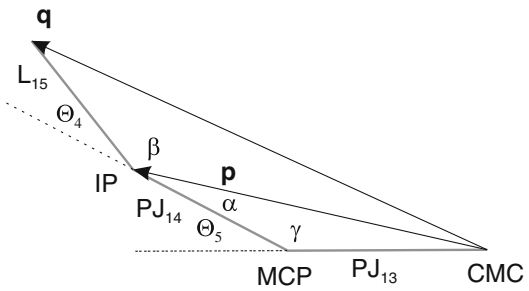

Fig. 4 Inverse kinematics of the thumb. Angles θ_4 and θ_5 in the MCP and IP joints are assessed by computing angles α, β, and γ

and DIP joints is not independent because the joints are coupled by ligaments, and so the estimate of f-e in the DIP joint can be obtained as follows:

$$\mathrm{DIP_{f\text{-}e}} = c \cdot \mathrm{PIP_{f\text{-}e}} \tag{5}$$

where $\mathrm{DIP_{f\text{-}e}}$ and $\mathrm{PIP_{f\text{-}e}}$ denote the angles of f-e in PIP and DIP joints. The simplification is valid for unconstrained finger movement. The correlation coefficients c were estimated as 0.32, 0.36, 0.16, and 0.25 for index, middle, ring, and little finger, respectively [11].

The kinematic structure of the thumb is more complicated than for fingers. The thumb is modeled as a serial manipulator with five DOF. In order to assess joint angles through inverse kinematics, the position and orientation of the fingertip are measured with the optical tracking system. The position $\mathbf{p}$ of the IP joint is calculated from the fingertip position $\mathbf{q}$, its orientation, and the length of the distal phalange L_{15}. Angles θ_4 and θ_5 in the MCP and IP joints are obtained by computing the angles α, β, and γ in the triangles depicted in Fig. 4. The side lengths of triangles are denoted by PJ_{13}, PJ_{14}, L_{15}, $|\mathbf{p}|$, and $|\mathbf{q}|$. The mechanism in Fig. 4 forms four different configurations:

$$\begin{aligned}
&\text{I.} && \Theta_4 > 0, \Theta_5 > 0; && \Theta_5 = \pi - (\alpha + \beta),\\
&\text{II.} && \Theta_4 < 0, \Theta_5 < 0; && \Theta_5 = (\alpha + \beta) - \pi,\\
&\text{III.} && \Theta_4 < 0, \Theta_5 > 0; && \Theta_5 = \pi - (\beta - \alpha),\\
&\text{IV.} && \Theta_4 > 0, \Theta_5 < 0; && \Theta_5 = (\beta - \alpha) - \pi
\end{aligned}$$

All except configuration III are natural for the thumb. Angles Θ_1, Θ_2, and Θ_3 are calculated from the system of trigonometric equations:

$$\mathbf{A}(\mathbf{A_4}\mathbf{A_5})^{-1} = \mathbf{A_1}\mathbf{A_2}\mathbf{A_3}, \tag{6}$$

as follows:

$$\theta_3 = \arctan_2\left(\frac{-a_z}{-s_z c_{45} - n_z s_{45}}\right), \tag{7}$$

$$\theta_1 = \arctan_2\left(\frac{n_y c_{45} - s_y s_{45}}{n_x c_{45} - s_x s_{45}}\right), \tag{8}$$

$$\theta_1 = \arctan_2\left(\frac{(-n_z c_{45} + s_z s_{45})(-s_3)}{a_z}\right). \tag{9}$$

Matrices $\mathbf{A_1}, \ldots, \mathbf{A_5}$ denote transformations between successive frames in the kinematic model of the thumb, while matrix $\mathbf{A}$ denotes the pose of the tip of the thumb (Fig. 1) with respect to the base frame. They are defined by the D-H parameters stated in Table 1. Function $\arctan_2 a/b$ is the four-quadrant arctan of elements a and b, while s_{45}, c_{45}, and s_3 denote $\sin(\Theta_4 + \Theta_5)$, $\cos(\Theta_4 + \Theta_5)$, and $\sin \Theta_3$, respectively.

2.5 Calibration of an instrumented glove

An optical goniometer built in the glove consists of an infrared light-emitting diode that directs light into an optical fiber (Fig. 5a). When the fiber is bent, a portion of the light beam is refracted out of the fiber. The reduced density of the light current is sensed by a phototransistor. The offset of the collector–emitter voltage is subtracted and the remainder amplified by an operational amplifier. The output voltage U_{AD} is transformed into a digital (raw) value.

One of the bend sensors was taken out of the glove and attached to two stiff segments linked with a hinge joint, in order to assess its input–output characteristics. Reflective markers were attached to both segments to measure the signals from the sensor and the corresponding bend angle simultaneously.

Optical sensors have low sensitivity at small bend angles. The sensitivity is increased with bend angle until it is stabilized (Fig. 5b). When sensors are already bent for extended fingers, the sensitivity does not change throughout the observed range of motion. An empirically chosen sum of two analytic functions was used to transform the DataGlove's raw response R into angle φ:

$$\varphi = k_1 + k_2 R + k_3 \ln(R - k_4). \tag{10}$$

Quasi-linear and polynomial approximations were also considered but did not perform well for extrapolation. During calibration, parameters k_1, k_2, k_3, and k_4 were estimated. The calculation was performed by least-squares error fit of the analytical function onto the experimentally assessed curve. The instrumented glove measures only relative angles of ab-ad, and therefore

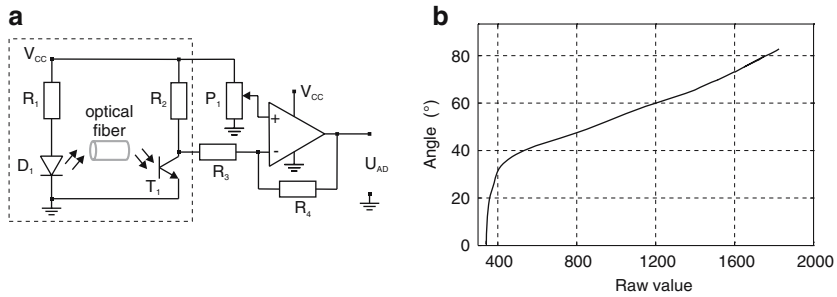

Fig. 5 Technical implementation of an optical goniometer (**a**), and its sensitivity (**b**) recorded for the sensor mounted onto two stiff segments linked with a hinge joint

the difference in ab-ad of index and middle fingers was used to calibrate the bend sensor between them.

3 Results

Four recordings of the simultaneous f-e of thumb and finger joints and four records of ab-ad of extended thumb and fingers were used to validate angles assessed through inverse kinematics and to assess the accuracy of the calibrated glove. The angles in finger and thumb joints were calculated using two different methods. Angles calculated from CoR were used as a reference in order to validate the accuracy of angles estimated through the method based on inverse kinematics. In the second part of our work we calibrated the glove with two different sets of angles. The first set was obtained by the reference method, and the second through inverse kinematics. Finally, joint angles measured with the calibrated glove were compared with the angles calculated by the reference method, to assess the accuracy of the glove calibrated with one of the two sets of angles.

The study was performed with a single subject. The trajectories of the CoR of joints were transformed to the coordinate frame attached to the hand dorsum. The lengths of finger and thumb segments were estimated as a byproduct of the CoR estimation. Their means and standard deviations are shown in columns I of Table 2.

The lengths of segments estimated from the CoR of joints are compared with the lengths calculated from the positions of markers recorded for the extended fingers (columns II), and with the lengths estimated by applying statistical anthropometry to the external dimensions of the hand (columns III). The results show that the lengths of finger segments estimated from the CoR of joints do not differ noticeably from the lengths that were obtained from statistical anthropometry and that were used to build the kinematic model of fingers, except for the proximal phalanx of the middle finger. In contrast, the differences between the lengths in columns II and III are evident. The differences between the lengths of thumb segments estimated from the CoR of joints and from statistical anthropometry are relatively high and can for some segments reach 8 mm. The large differences are most probably related to the methodology used to determine anthropometric scaling factors describing the lengths of thumb segments with respect to the external dimensions of the hand. The anatomy of the thumb was, namely, described in 2D, from X-ray images [4].

Table 2 Lengths of finger segments, estimated from the CoR of joints (I), from position of surface markers (II), and from statistical anthropometry (III)

$\overline{L} \pm \sigma$ (mm)	I	II	III
Thumb			
L_{metacarp}	44.8 ± 1.1	40.9 ± 2.4	51.2
L_{prox}	35.0 ± 0.9	36.3 ± 3.5	40.0
L_{dist}	24.5 ± 1.1	23.4 ± 2.4	32.2
Index f.			
L_{prox}	47.4 ± 0.7	41.3 ± 0.9	45.5
L_{mid}	25.4 ± 0.6	34.2 ± 0.4	26.0
L_{dist}	23.8 ± 0.1	20.1 ± 0.2	23.0
Middle f.			
L_{prox}	50.0 ± 0.5	52.0 ± 0.9	42.0
L_{mid}	30.8 ± 0.9	31.3 ± 0.4	30.9
L_{dist}	24.6 ± 0.1	22.8 ± 0.4	25.9

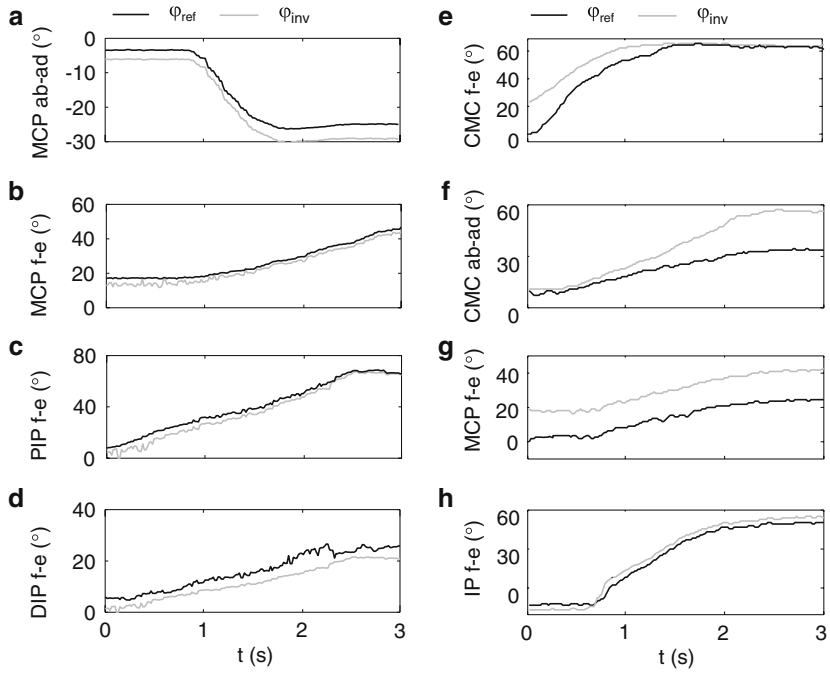

Fig. 6 Ab-ad of MCP joint (**a**), f-e of MCP (**b**), PIP (**c**), and DIP (**d**) joints of the index finger, f-e of CMC (**e**), ab-ad of the CMC joint (**f**) and f-e of the MCP (**g**) and IP (**h**) joints of the thumb estimated from the CoR of joints (black line) and through inverse kinematics (gray line)

Table 3 Mean and standard deviation of the difference between the reference angles and angles estimated through inverse kinematics for thumb, index, and middle fingers

$\overline{\Delta\varphi} \pm \sigma\,(^\circ)$	Thumb	$\overline{\Delta\varphi} \pm \sigma\,(^\circ)$	Index f.	Middle f.
CMC f-e	-6.6 ± 7.4	MCP ab-ad	3.4 ± 0.7	-0.8 ± 1.1
CMC ab-ad	-12.4 ± 8.9	MCP f-e	2.4 ± 0.9	6.6 ± 0.9
MCP f-e	-17.5 ± 1.3	PIP f-e	7.9 ± 4.7	3.9 ± 1.4
IP f-e	0.6 ± 4.0	DIP f-e	6.7 ± 4.4	7.9 ± 8.2

The angles in the joints of thumb and index finger, presented in Fig. 6, were assessed from the CoR of joints (black line, φ_{ref}) and through the inverse kinematics (grey line, φ_{inv}). The mean difference between the angles estimated through inverse kinematics and the reference angles estimated from the CoR of joints, and the standard deviation of the difference, are presented in Table 3 for the thumb, index, and middle fingers. The mean difference between ab-ad angles of fingers estimated with the reference method and through inverse kinematics did not exceed 4° in any instance. The reference angle of f-e in the MCP joint and the same angle obtained through inverse kinematics were comparable for the index finger, while for the middle finger the mean difference between these angles reached 6.6°. This deviation was caused by the length of the proximal phalanx that was used to build the kinematic model of the middle finger. The length of the proximal phalanx of the middle finger (Table 2) obtained from statistical anthropometry differs noticeably from the length estimated from the CoR of joints. When the inverse-kinematics equations were solved for the updated model, based on the lengths of finger segments obtained from the CoR of joints, the difference was reduced to less than 3°.

Angles in the DIP joints of the index and middle fingers were estimated from the f-e angles of PIP joints by applying Eq. 5. Joint angles in the PIP and DIP joints

reconstructed through inverse kinematics are smaller than the reference angles for the index finger as well as for the middle finger. The difference originates from the position of the marker, which cannot be placed in the CoR of the DIP joint but has to go above this joint. As a consequence, the angles estimated for PIP joints are smaller. Angles in the DIP joints were not used to calibrate the glove because the glove did not have bend sensors to measure flexion of the distal joints. They were estimated anyway, to demonstrate that angles in the DIP joints could indeed be estimated from the angles of PIP joints for unconstrained finger movement.

When it was applied to the thumb, the inverse-kinematics method did not give results that were as promising as for fingers. The angles of f-e of the CMC and f-e of the IP joints were acquired with mean error $-6.6°$ and $0.6°$, respectively. The mean difference between the reference angles and the angles calculated through inverse kinematics was larger than $17°$ and $12°$ for the f-e angle of the MCP joint and the ab-ad angle of the CMC joint. Standard deviations were notable for the CMC joint, in which they exceeded $7°$. The time courses of angles in the CMC joint in Fig. 6 (panels e, f) show that the error in the f-e angle assessed through inverse kinematics decreases with flexion, and the error in the ab-ad angle increases with the adduction of the thumb. This indicates that the CoR of the CMC joint and its axes of rotation were not chosen in an optimal manner when developing a kinematic model of the thumb. Such an optimal choice was in fact not even possible. The exact location of the center of rotation and the directions of axes of rotation of the CMC joint could not be estimated from anthropometric data of the hand that are obtained in 2D. However, the large mean error (and small standard deviation) estimated for the f-e angle of the MCP joint originates from the erroneously calculated orientation of the distal phalange. The reflective marker was attached to the thumbnail, which is not parallel to the distal phalange. As a result, the position of the IP joint $\mathbf{p}$ was miscalculated from the fingertip position $\mathbf{q}$ and orientation (Fig. 4).

The accuracy of the glove is presented in Figs. 7–9. In Fig. 7 the angles obtained with the reference method from the CoR of joints ($\varphi_{\text{ref calib}}$), and in Fig. 8 the angles acquired with the inverse kinematics method ($\varphi_{\text{inv calib}}$), were used to calibrate the glove. The angles of relative ab-ad between the index and middle fingers and f-e in the MCP and PIP joints of the index finger are shown on the left panels a, b, and c, respectively. The dashed lines represent the angles used to calibrate the glove ($\varphi_{\text{ref calib}}$ or $\varphi_{\text{inv calib}}$). The full grey lines ($\varphi_{\text{glove}}$) represent the analytic functions (10) obtained as a result of calibration. They illustrate the uniform transformations of the glove's raw responses into angles. The four sets of reference angles ($\varphi_{\text{ref valid}}$), which were used for validation, are plotted as functions of raw responses of the glove with full black lines. Errors in the right panels represent the difference between angles estimated with the reference method ($\varphi_{\text{ref valid}}$) and angles assessed with the calibrated glove (φ_{glove}).

The accuracy of the glove calibrated with the reference angles is limited to $\pm 5°$ (Fig. 7), and it cannot be significantly improved for the instrumented gloves that include optical bend sensors having low sensitivity at small bend angles. The results of the calibration with the angles obtained by the inverse-kinematics method are presented for the index finger in Fig. 8. The angles of finger joints were calculated from the positions of markers above the DIP joint. The best accuracy was obtained for f-e of the MCP joint and is comparable to the accuracy obtained when the angles estimated with the reference method were used to calibrate the glove. The mean errors of the f-e angle of the PIP joint as well as of the relative ab-ad angle between the index and middle fingers did not exceed $7°$.

The model-based method for assessing angles in the joints of the thumb through inverse kinematics did not provide any relevant advantage over the reference method in terms of the number of markers. For this reason, only the angles estimated by the reference method were used to calibrate the glove. The accuracy of the calibrated glove for the thumb is presented in Fig. 9. The glove did not have a sensor to measure the f-e of the MCP joint. The mean error between the reference angles and the angles obtained from the calibrated glove for the thumb did not exceed $3°$. Moreover, the difference rarely left the interval $[-5°, 5°]$.

Mean differences between the four sets of reference angles, which were calculated from the CoR of joints, and the angles acquired from the calibrated glove are presented with accompanying standard deviations in Table 4. Values in the second and third columns are related to the calibration of the glove with the angles obtained with the reference method. The results of the calibration with the inverse-kinematics method are presented in the fourth and fifth columns, but only for the

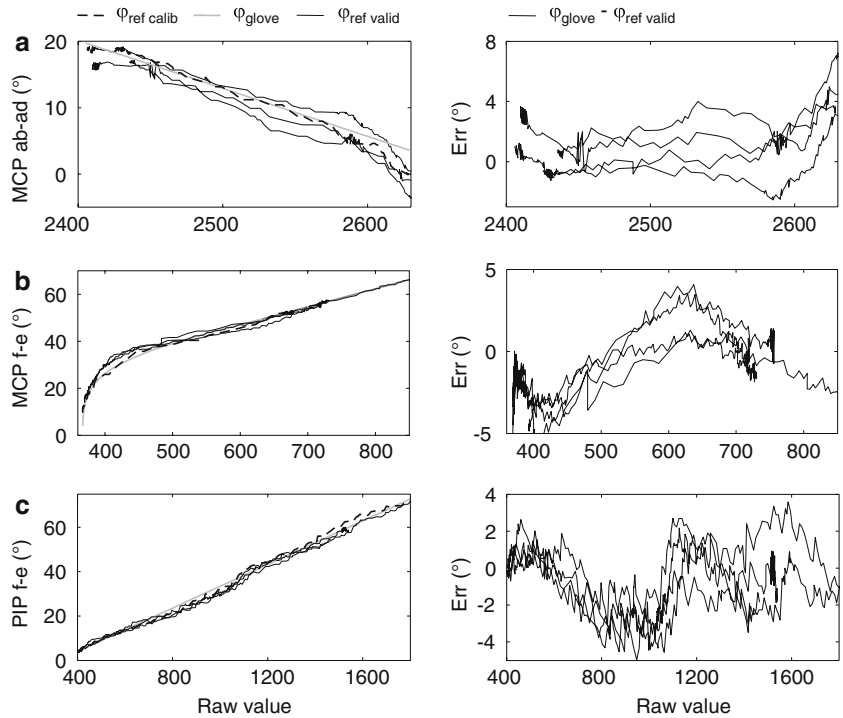

Fig. 7 Accuracy of the glove, calibrated with the reference method ($\varphi_{\text{ref calib}}$): relative ab-ad between the index and middle fingers (**a**), f-e of MCP (**b**) and PIP (**c**) joints of the index finger. Right panels: the difference between the reference angles ($\varphi_{\text{ref valid}}$) and the angles measured with the calibrated glove (φ_{glove})

index and middle fingers. The glove measures only the relative angles of ab-ad between the index and middle fingers, and therefore only two values are stated.

4 Summary and conclusions

In this paper, a simple method for assessing angles in thumb and finger joints, which is appropriate for the calibration of an instrumented glove, was proposed. The method is based on an optical tracking system and a kinematic model of the hand. It requires one marker per finger and three on the dorsal aspect of the hand to calculate the angles in finger joints. A further three markers are required to calculate angles in the thumb joints. The accuracy of the method and the calibrated glove were estimated by a reference method with multiple markers in which joint angles are calculated from their CoR. The methods estimating the CoR [16,23] of MCP, PIP, DIP, and IP joints of thumb and fingers were also improved. A weighted average was introduced into the cost functions presented in Eqs. 2 and 3 that have been proposed in the literature to assess parameters of CoR of joints. This modification made them more robust for practical applications when speed of motion in joints is varying with bend angle.

Five markers, required in order to estimate the angles in the index- and middle-finger joints through inverse kinematics, were attached to the capitate bone, two above the MCP joints and two above the DIP joints. Because PIP and DIP joints were kept still during f-e of MCP joints, we were able to reconstruct the CoR of MCP joints using the same set of five markers. In this way, the exact positioning of the coordinate systems attached to the finger bases were obtained. The marker attached to the capitate bone was used to position the hand model in 3D space. Exact positioning of the base of each finger was essential for a reliable solution of the inverse kinematics.

The thumb was modeled with a universal joint and two hinge joints, and therefore three additional markers were necessary to assess angles in the thumb through inverse kinematics. The CoR of the CMC joint and its

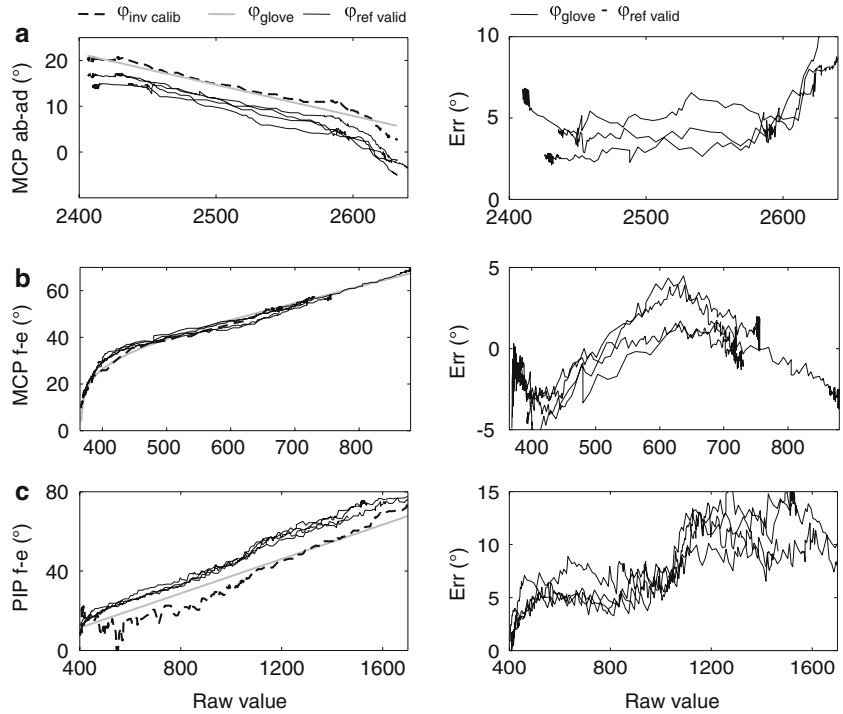

Fig. 8 Accuracy of the glove, calibrated with the inverse-kinematics method ($\varphi_{\text{inv calib}}$): relative ab-ad between index and middle fingers (**a**), f-e of MCP (**b**) and PIP (**c**) joints of the index finger. Right panels: the difference between the reference angles ($\varphi_{\text{ref valid}}$) and the angles measured with the calibrated glove (φ_{glove})

Table 4 Accuracy of the instrumented glove: mean and standard deviation of the difference between the reference angles and the angles measured with the glove calibrated with the reference and inverse-kinematics method

$\overline{\Delta\varphi} \pm \sigma\,(^\circ)$	Reference method		Inverse-kinematics method	
	Index f.	Middle f.	Index f.	Middle f.
MCP ab-ad	1.5 ± 1.7		5.3 ± 2.2	
MCP f-e	-1.5 ± 1.5	-1.2 ± 1.6	-1.1 ± 1.6	4.5 ± 2.2
PIP f-e	-0.6 ± 1.4	4.0 ± 3.56	6.1 ± 5.13	6.7 ± 6.3
	Reference method			
$\overline{\Delta\varphi} \pm \sigma\,(^\circ)$	Thumb			
CMC f-e	0.8 ± 3.0			
CMC ab-ad	2.4 ± 4.3			
IP f-e	-1.7 ± 2.3			

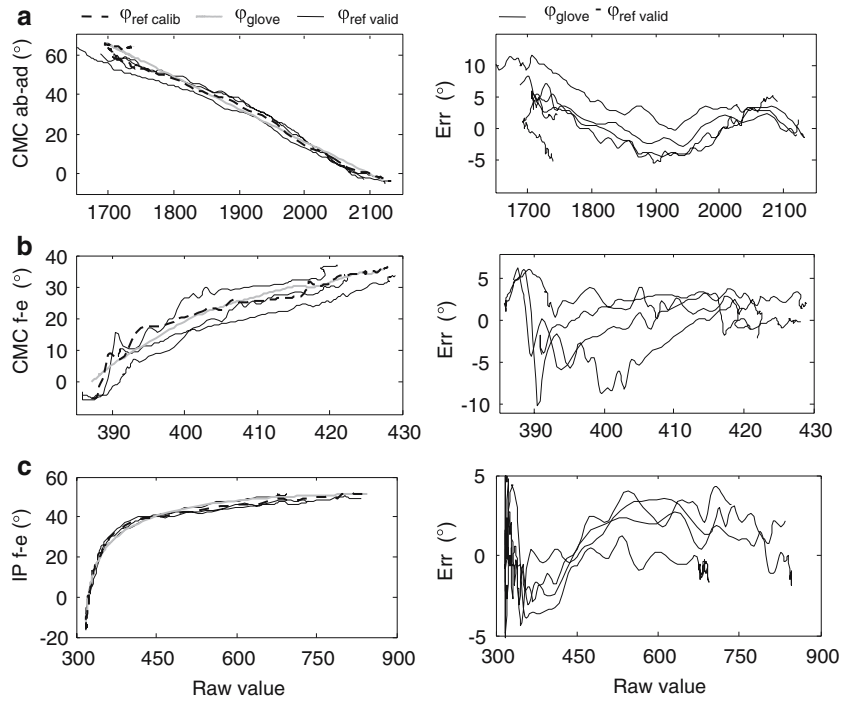

Fig. 9 Accuracy of the glove, calibrated with the reference method ($\varphi_{\text{ref calib}}$): relative ab-ad (**a**) and f-e (**b**) of the CMC joint and f-e of the IP (**c**) joint of the thumb. Right panels: the difference between the reference angles ($\varphi_{\text{ref valid}}$) and the angles measured with the calibrated glove (φ_{glove})

axes of rotation were not chosen in an optimal manner. In a similar way, the orientation of the distal phalange could not be calculated accurately from the position of markers attached above the IP joint and on the thumbnail. Moreover, the lengths of some segments of thumb obtained from the CoR of joints and from the statistical anthropometry differed by almost 8 mm. These inaccuracies altogether resulted in large mean differences between the reference angles and the angles assessed through inverse kinematics, particularly for ab-ad of the CMC (12.4°) and f-e of the MCP (17.5°) joint. The reference method used four markers to assess the angles in the thumb, but required only one more marker than the inverse-kinematics method in order to assess angles in thumb joints with notably better accuracy. However, a set of predefined movements have to be recorded in advance to determine the parameters that are required to reconstruct the CoR of joints from the position of markers attached to the thumb. Despite that, we considered the reference method as more appropriate for calibrating the glove for the thumb.

The reference angles and the angles obtained by the proposed model-based method were used to study the accuracy of the instrumented glove for fingers, while in the case of the thumb only the reference angles were used to calibrate the glove. The best accuracy that can be expected from the glove, when all systematic errors are reduced to a minimum, is limited by the physical properties of its bend sensors. Validation of the angles obtained with the calibrated glove against the reference method showed that the gloves implemented with optical goniometers cannot measure joint angles with an accuracy better than ±5°. The overall accuracy could probably not be significantly improved by choosing a different type of bend-angle sensing (resistive or inductive).

The method for assessing joint angles through inverse kinematics was used only to calibrate the optical goniometers that measured the angles in finger joints. A systematic error that can be attributed to the inverse-kinematics method worsened the accuracy of the glove. It reached ±5.3° in the case of MCP joints. Larger

systematic errors were estimated for f-e of PIP joints and relative ab-ad between the index and middle fingers, but they did not exceed 7° in any instance. One can argue that angles in finger joints need not to be measured accurately because in telemanipulation systems large kinematic errors can be compensated for by visual feedback. However, when the glove is used for precise rendering of hand gestures or when studying the control of the human hand, accurate assessment of angles in finger joints is vital. The calibrated glove will be employed in future work to evaluate the quality of grasp of both healthy and impaired subjects performing dexterous manipulation of an object.

Acknowledgements This work was supported by Slovenian Research Agency. The authors thank Gregorij Kurillo for reviewing the manuscript and his advice during the work.

References

1. Allevard T, Benoit E, Foulloy L (2005) Dynamic gesture recognition using signal processing based on fuzzy nominal scales. Measurement 38(3):303–312
2. Bernardin K, Ogawara K, Ikeuchi K, Dillmann R (2005) A sensor fusion approach for recognizing continuous human grasping sequences using hidden Markov models. IEEE Trans Robot Autom 21(1):47–57
3. Bicchi A (2000) Hands for dexterous manipulation and robust grasping: a difficult road toward simplicity. IEEE Trans Robot Autom 9(4):432–443
4. Buchholz B, Armstrong T, Goldstein S (1992) Anthropometric data for describing the kinematics of the human hand. Ergonomics 35(3):261–273
5. Chang L, Matsuoka Y (2006) A kinematic thumb model for the ACT hand. In: Proceedings of international conference on robotics and automation. Orlando, FL, pp 1000–1005
6. Chang L, Pollard N (2006) Constrained least-squares optimization for robust estimation of center of rotation. J Biomech 40(6):1392–1400
7. Denavit J, Hartenberg R (1955) A kinematic notation for lower-pair mechanisms based on matrices. J Appl Mech 22:215–221
8. Dipietro L, Sabatini A, Dario P (2003) Evaluation of an instrumented glove for hand-movement acquisition. J Rehabil Res Dev 40(2):179–190
9. Gamage S H U, Lasenby J (2004) New least squares solution for estimating the average centre of rotation and the axis of rotation. J Biomech 35(1):87–93
10. Halvorsen K, Lesser M, Lundberg A (1999) A new method for estimating the axis of rotation and the center of rotation. J Biomech 32(11):1221–1227
11. Kamper D, Cruz E, Siegel M (2003) Stereotypical fingertip trajectories during grasp. J Neurophysiol 90(6):3702–3710
12. Klopcar N, Jadran L (2005) Kinematic model for determination of human arm reachable workspace. Meccanica 40(2):203–219
13. Kramer J (1996) Determination of thumb position using measurements of abduction and rotation. US Patent 5:482,056
14. Laszlo L, Gabor S (2003) Dynamics of digital force control applied in rehabilitation robotics. Meccanica 38(2):213–226
15. MacKenzie L, Iberall T (1994) The grasping hand. Elsevier Science, Amsterdam
16. Miyata N, Kouchi M, Kurihara T, Mochimaru M (2004) Modeling of human hand link structure from optical motion tracking data. In: Proceedings of international conference on intelligent robots and systems. Sendai, Japan, pp 2129–2136
17. Okamura A, Smaby N, Cutkosky M (2000) An overview of dexterous manipulation. In: Proceedings of international conference on robotics and automation San Francisco, CA, pp 255–262
18. Sciavicco L, Siciliano B, (2002) Modelling and control of robot manipulators. Springer-Verlag
19. Sturman D, Zeltzer D (1994) A survey of glove-based input. IEEE Comput Graph Appl 14(1):30–39
20. Vamplew P (1996) Recognition of sign language using neural networks. Ph.D. Thesis, School of Computing, University of Tasmania
21. Veber M, Bajd T, Munih M (2006) Assessment of finger joint angles and calibration of instrumental glove. In: Advances in robot kinematics. Ljubljana, Slovenia
22. Williams N, Penrose J, Caddy C, Barnes E, Hose D, Harley P (2000) A goniometric glove for clinical hand assessment construction, calibration and validation. J Hand Surg 25(2):200–207
23. Zhang X, Lee S -W, Braido P (2003) Determining finger segmental CoR in flexion-extension based on surface marker measurement. J Biomech 36(8):1097–1102